Geophysical Research Letters

RESEARCH LETTER
10.1029/2018GL079778

Key Points:
- First in situ observation of reconnection between an earthward propagating FR and the geomagnetic field
- This is a highly deformed FR with its leading part being eroded by the reconnection
- MMS crossed the diffusion region of this reconnecting current sheet

Correspondence to:
M. Zhou,
monmentum82@gmail.com

Citation:
Man, H. Y., Zhou, M., Deng, X. H., Fu, H. S., Zhong, Z. H., Chen, Z. Z., et al. (2018). In situ observation of magnetic reconnection between an earthward propagating flux rope and the geomagnetic field. *Geophysical Research Letters*, *45*, 8729–8737. https://doi.org/10.1029/2018GL079778

Received 27 JUL 2018
Accepted 14 AUG 2018
Accepted article online 28 AUG 2018
Published online 6 SEP 2018

In Situ Observation of Magnetic Reconnection Between an Earthward Propagating Flux Rope and the Geomagnetic Field

H. Y. Man[1,2], M. Zhou[2], X. H. Deng[2], H. S. Fu[3], Z. H. Zhong[2,4], Z. Z. Chen[3], C. T. Russell[5], R. J. Strangeway[5], W. R. Paterson[6], B. L. Giles[6], P.-A. Lindqvist[7], R. E. Ergun[8], and J. L. Burch[9]

[1]Department of Physics, School of Science, Nanchang University, Nanchang, People's Republic of China, [2]Institute of Space Science and Technology, Nanchang University, Nanchang, China, [3]School of Space and Environment, Beihang University, Beijing, China, [4]School of Resources Environmental and Chemical Engineering, Nanchang University, Nanchang, China, [5]Department of Earth, Planetary and Space Sciences, University of California, Los Angeles, CA, USA, [6]NASA, Goddard Space Flight Center, Greenbelt, MD, USA, [7]Royal Institute of Technology, Stockholm, Sweden, [8]University of Colorado LASP, Boulder, CO, USA, [9]Southwest Research Institute, San Antonio, TX, USA

Abstract It has been proposed that, in the near-Earth magnetotail, earthward propagating flux ropes can merge with the Earth's dipole magnetic field and dissipate its magnetic energy. However, the reconnection diffusion region related to this process has not been identified. Here we report the first in situ observation of magnetic reconnection between an earthward propagating flux rope and the closed magnetic field lines connecting to Earth. Magnetospheric Multiscale (MMS) spacecraft crossed a vertical current sheet between the leading edge of the flux rope (negative B_z) and the geomagnetic field (positive B_z). The subion-scale current sheet, super-Alfvénic electron outflow, Hall magnetic and electric field, conversion of magnetic energy to plasma energy ($J \cdot E > 0$), and magnetic null were observed during the crossing. All the above signatures indicate that MMS detected the reconnection diffusion region. This result is also relevant to other planets with intrinsic magnetosphere.

Plain Language Summary Magnetic reconnection is an essential source process in space weather. Reconnection produces many magnetic structures, such as the magnetic flux ropes and reconnection fronts, and ejects them away from the reconnection site. These structures interact with the surrounding space environment during its propagation, which may have great geomagnetic effects. A highly asymmetric earthward propagating magnetic flux rope is often observed in the Earth's magnetotail. It has long been suggested that this asymmetrical magnetic flux rope is formed due to the flux erosion of the earthward part of the flux rope by magnetic reconnection between the flux rope and the geomagnetic field. Despite various theoretical and numerical simulation studies, there has been no observational evidence to confirm this scenario. This paper reports the first observation of magnetic reconnection occurring at the earthward front of a flux rope in the Earth's magnetotail, confirming the previous theoretical predictions and explaining the formation of the asymmetric flux rope which is often observed in the near-Earth magnetotail.

1. Introduction

Magnetic flux ropes (MFRs), which have frequently been observed in space plasmas throughout the solar system, are coherent structures consisting of helical magnetic field lines. They are believed to be produced by magnetic reconnection and are important for mass, magnetic flux, and energy transport in space weather (Dere et al., 1999; Lepping et al., 1990; Russell & Elphic, 1979; Zong et al., 2004; Zhang et al., 2012). Tremendous efforts have been made in the past few decades to understand the formation, evolution, and dissipation of MFRs. It is well known that multiple X line reconnection due to the tearing instability can produce MFR (Deng et al., 2004; Lee & Fu, 1985). Secondary MFR, with the scale on the order of the ion inertial length, can be formed in an electron-scale current sheet due to the secondary tearing instability (Daughton et al., 2006; Drake et al., 2006; Fu et al., 2013, 2017; Huang et al., 2012; Wang et al., 2010). On the other hand, recent simulations and observations confirm that electron Kelvin-Helmholtz instability can generate secondary MFR by forming electron vortex (Fermo et al., 2012; Huang, Lu, et al., 2015; Zhong et al., 2018). MFRs can coalesce to form larger MFRs, during which energy is dissipated and particles are

energized (Wang et al., 2016; Zhou, Pang, et al., 2014; Zhou et al., 2017). Magnetic cloud in the solar wind, the prototype of which is MFR, may reconnect with the solar wind magnetic field around it and erode its magnetic flux (Ruffenach et al., 2012).

The fate of earthward propagating MFRs in the Earth's magnetotail is a longstanding problem. Slavin et al. (2003) proposed the idea of "re-reconnection" that earthward moving MFRs may reconnect with the geomagnetic field and dissipate the magnetic energy stored in their earthward portion. Such process is later confirmed in the simulation of Huang, Zhou, et al. (2015), and is considered to be important for triggering magnetospheric substorms (Ma & Lu, 2009; Winglee et al., 2009). Dissipation of the leading part of the MFR may lead to the highly asymmetric MFR, or dipolarization front which is quite common in the near-Earth tail (Fu et al., 2012; Lu et al., 2015; Runov et al., 2009; Vogiatzis et al., 2015; Zhou et al., 2009). Nevertheless, the in situ evidence for the reconnection diffusion region of this scenario is missing.

In this letter, we present MMS observations of magnetic reconnection that occurred between an MFR and the closed magnetic field lines in the near-Earth magnetotail. Unprecedented high resolution (approximately millisecond) and high-quality data from the MMS mission have been used in this study (Burch et al., 2016). Specifically, the Fluxgate Magnetometer provides 3-D magnetic field measurements (Russell et al., 2016), the Electric field Double Probe provides 3-D electric field measurements (Ergun et al., 2016; Lindqvist et al., 2016), and the Fast Plasma Instrument provides 3-D ion and electron velocity distributions and the integrated plasma moments (Pollock et al., 2016).

2. Observations

Figure 1 displays the observations of MMS1 from 18:50 to 19:05 UT on 14 August 2017, when MMS satellite was in the Earth's magnetotail around [−18.5, 15.5, 1.3] R_E (Earth radii) in geocentric solar magnetospheric coordinate system. During the time interval, the four MMS spacecraft were flying in a regular tetrahedron formation with an average separation of 27 km, which is approximately two electron inertial lengths in the quite plasma sheet (d_e~12 km for a plasma number density of 0.2 cm^{-3} between 19:03 and 19:04 UT).

MMS was outside the plasma sheet before 18:53:30 UT. Magnetic field was northward and deflected dawnward because MMS was near the dusk flank of the magnetotail. MMS entered the plasma sheet at around 18:53:30 UT as it observed a decrease of magnetic field strength and the emergence of hot plasma sheet population, which is manifested as enhancement in the ion omniflux from 300 eV to 25 keV, and electron omniflux from 100 eV to 10 keV. In addition, the ion plasma β increased from less than 1 to nearly 10. From 18:56:00 to 18:57:30 UT, MMS detected a tripolar B_z variation from positive to negative and then to positive (Figure 1a), within an earthward ion bulk flow with a peak speed at about 200 km/s (Figure 1d). The ion number density, plasma β, and flow speed may be underestimated because there are significant fluxes of energetic ions with energies higher than the upper limit of the Fast Plasma Instrument. The latter negative-to-positive bipolar variation of B_z is asymmetric in both the amplitude and duration: negative B_z had a minimum value of about −6 nT and persisted for about 20 s, while positive B_z had a maximum value of about 10 nT and was followed by a prolonged interval (~5 min) of gradual B_z decrease. The rapid increase of B_z resembles the well-known dipolarization front, as the ion density decreases across this structure. This highly asymmetric B_z structure is also likely a deformed earthward moving MFR, with its leading part being dissipated. Since B_x was quite small during the entire crossing of the bipolar structure, the asymmetric B_z observed by MMS was not due to the oblique trajectory of MMS across the MFR. Instead, it implies the asymmetric nature of this MFR along its moving direction.

It is interesting to note that the MFR was preceded by a positive B_z. The transition from the positive to the negative B_z is sharp (peak-to-peak duration was less than 5 s). This indicates that a thin current sheet was in association with the variation of B_z from positive to negative. The positive B_z was in the closed field lines that connected to Earth since thermal electrons were isotropic (Figure 1h). Thus, this current sheet was formed between the geomagnetic field and the deformed MFR.

Figure 2a illustrates a schematic view of the MMS trajectory across the deformed MFR and the closed field lines in the *x*-*z* plane. To examine the current sheet between the MFR and the closed field lines in detail, we constructed a local LMN coordinate system by applying the minimum variance analysis (Sonnerup & Scheible, 1998) on the magnetic field measured by MMS1 between 18:55:35 and 18:55:40 UT. Relative to

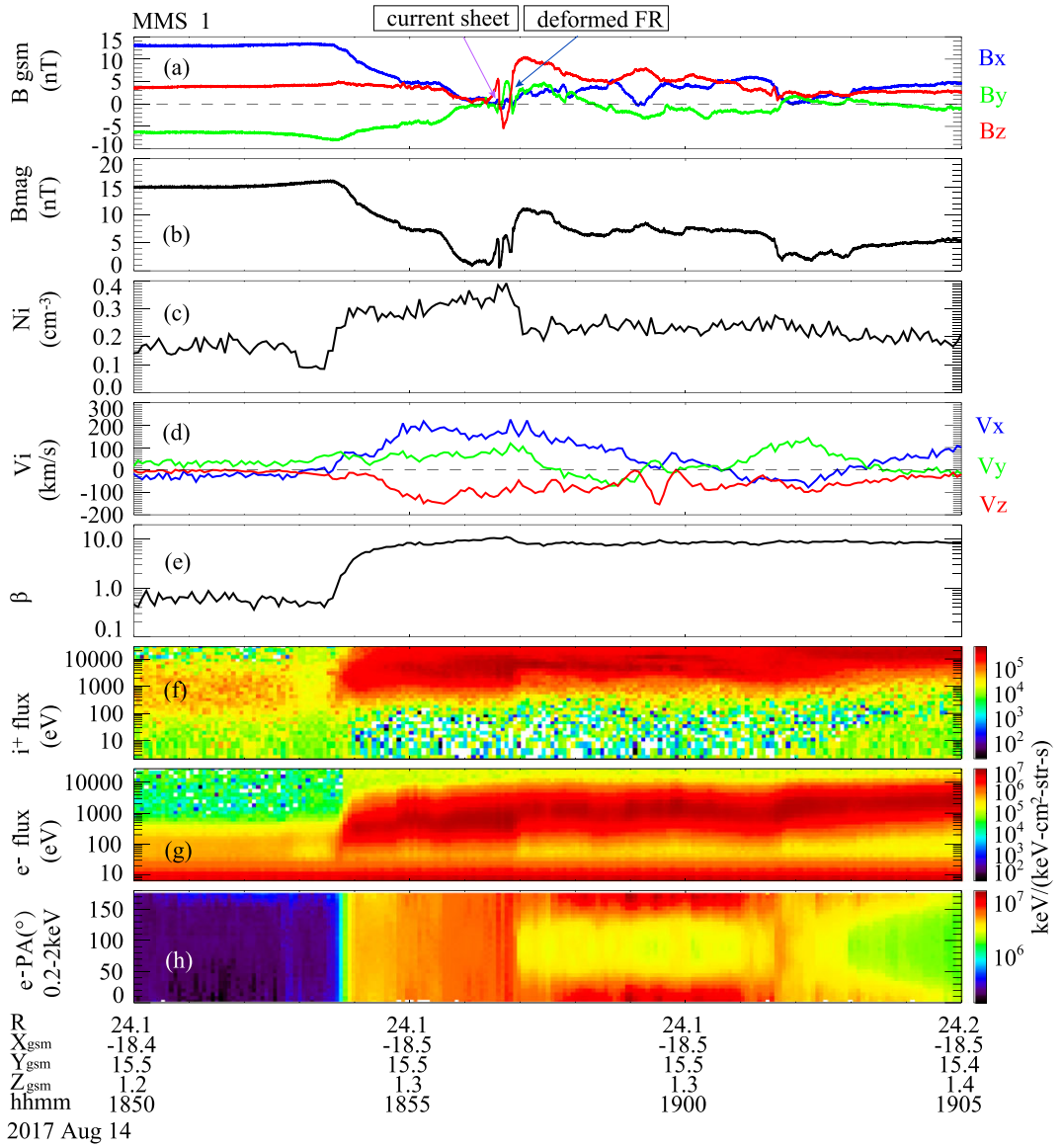

Figure 1. Overview of MMS1 observations between 18:50 and 19:05 UT. (a) Three components of magnetic fields; (b) magnetic field strength; (c) ion number density; (d) ion bulk velocity; (e) ion plasma β defined as $\beta = n_i k_B T_i/(B^2/2\mu_0)$, where n_i is the ion density, k_B is the Boltzmann constant, T_i is the ion temperature, B is the magnetic field strength, and μ_0 is the free space permeability; (f) ion and (g) electron omnidirectional differential energy flux; and (h) pitch angle distribution of electrons from 0.2 to 2 keV. Vectors are displayed in GSM coordinate system.

geocentric solar magnetospheric coordinates, **N** = [0.9759, 0.1160, −0.1847] is the current sheet normal and is positive toward the Sun; **L** = [0.2061, −0.2128, 0.9551] is tangential to the current sheet and points to the maximum variance direction; and **M** = [0.0715, −0.9702, −0.2316] completes the right-handed orthogonal system and is mainly in the negative **Y** direction, that is, **M** = **N** × **L**. In addition, we calculated the normal direction of the current sheet by using the multispacecraft timing analysis (Russell et al., 1983). The derived normal direction is consistent with the **N** obtained from minimum variance analysis. Moving speed of the current sheet along the normal was about 240 km/s, which is close to the ion bulk velocity in the normal direction (Figure 3c). Having known the observational duration of the current sheet (~0.4 s), we estimate the thickness of the current sheet as 100 km~0.28 d_i~12 d_e; here d_i~360 km is the ion inertial length and d_e~8 km is the electron inertial length based on the plasma number density of 0.4/cm^3 upstream (inflow) of the current sheet. This is essentially a vertical current sheet because the current sheet normal was mainly in the X_{GSM} direction.

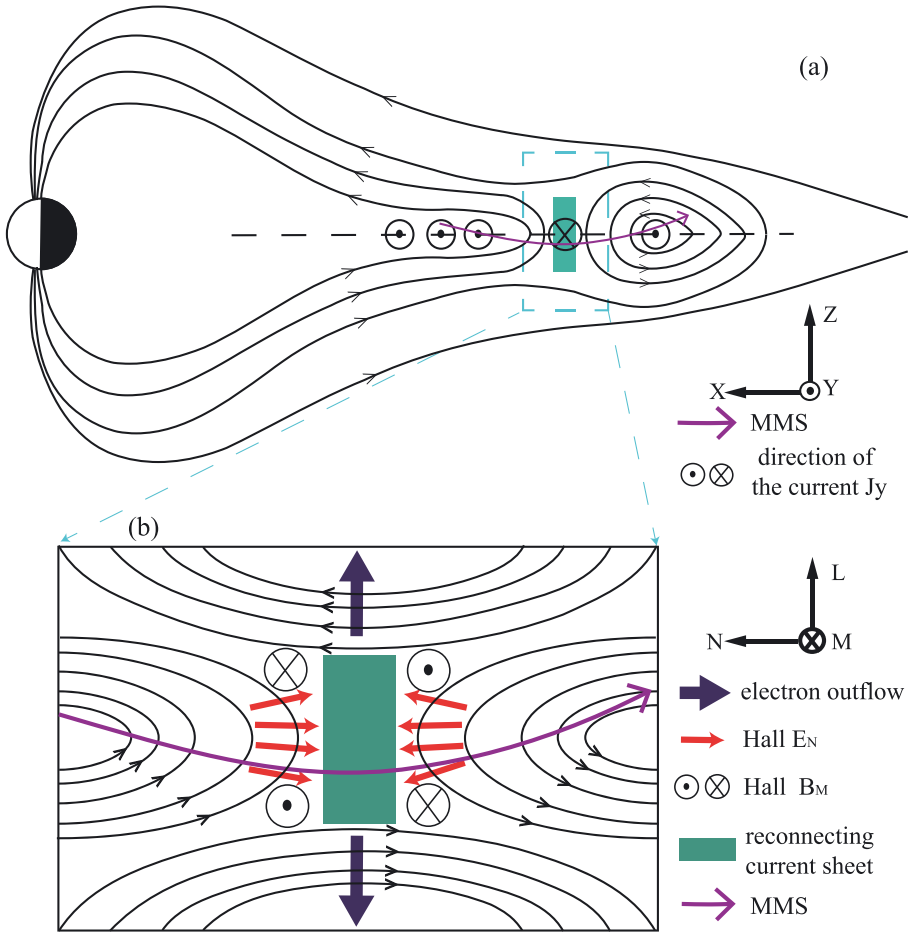

Figure 2. Schematics of MMS trajectory across the reconnection region between the MFR and the geomagnetic field. (a) large-scale view in the *x-z* plane in GSM coordinates. (b) Zoomed-in view of the reconnection diffusion region in the L-N plane in LMN coordinate system. The LMN coordinate system is defined in the main text.

Figure 3e shows that the current enhancement (~50 nA/m^2) corresponding to the reversal of B_L was opposite to the duskward cross-tail current in the plasma sheet. This positive J_M was primarily contributed by the electron current since the current was mainly carried by electrons flowing in the $-\mathbf{M}$ direction as ion flow V_{iM} was merely −50 km/s inside the current sheet. The following evidence strongly suggests that this vertical current sheet was reconnecting.

A negative outflow electron jet V_{eL} was observed by MMS within the current sheet. It corresponds to a negative B_N, which is consistent with the 2-D reconnection geometry depicted in Figure 2b. The jet speed was about 500 km/s and was much larger than the upstream ion Alfvén speed ~210 km/s based on the upstream magnetic field of 6 nT and plasma density of 0.4/cm^3. This super-Alfvénic electron outflow jet exists close to the X line and has been used as an evidence for identifying an X line (Shay et al., 2007; Zhou, Deng, et al., 2014, 2018).

Figures 3a and 3f demonstrate the existence of Hall magnetic field and electric field expected from the collisionless Hall reconnection (Birn et al., 2001; Drake et al., 2008). Magnetic field B_M shows a negative-to-positive variation as MMS1 moved from the dipole field to the MFR, as indicated by the change of B_L from positive to negative. Normal electric field E_N changes from negative to positive as B_L changes from positive to negative. This is consistent with a converging Hall electric field pointing toward the reconnecting current sheet in the ion diffusion region (e.g., Borg et al., 2005). We note that the Hall magnetic field B_M is asymmetric as the negative B_M occupies a larger area than the positive B_M, and the negative B_M has a larger magnitude than the positive B_M. This asymmetry may be caused by the slightly asymmetric asymptotic magnetic field B_L of the current sheet.

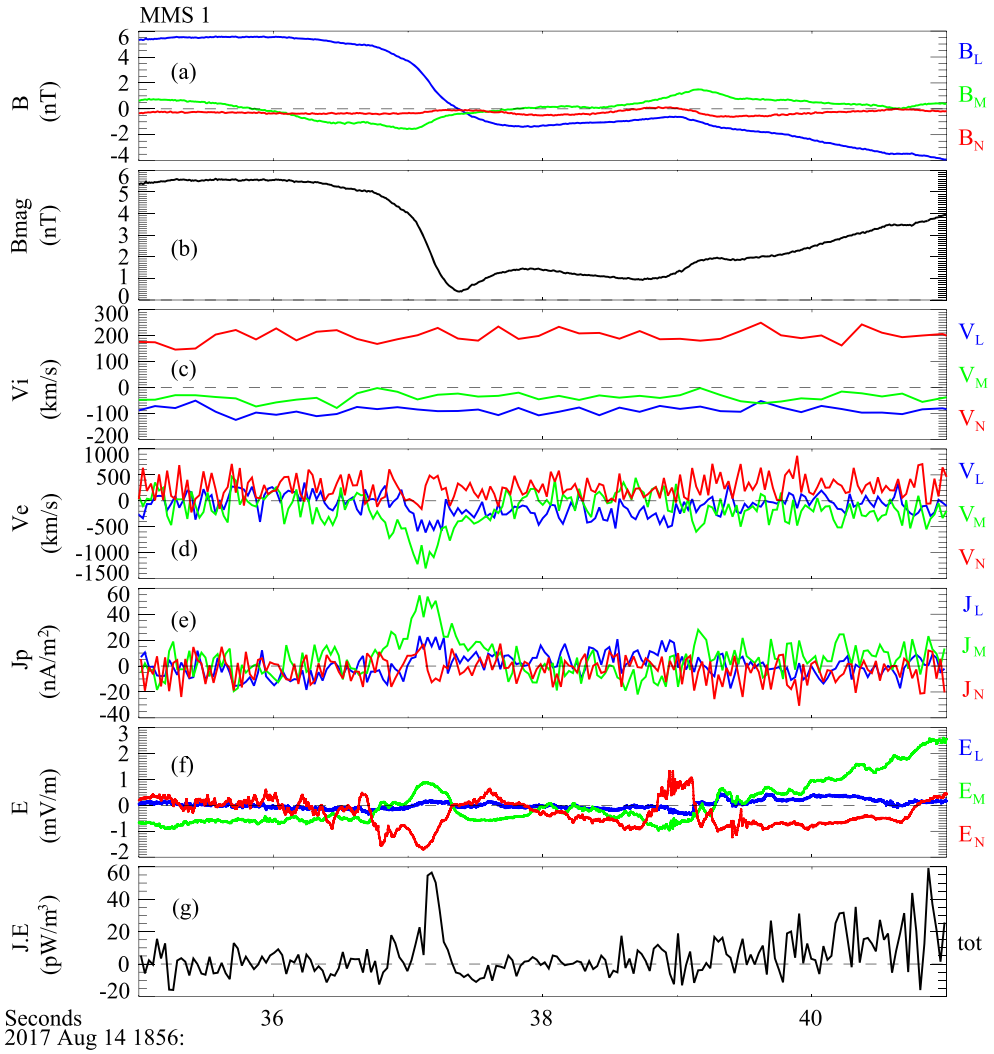

Figure 3. MMS1 observations of the reconnection diffusion region between 18:56:35 and 18:56:41 UT. (a) Three components of magnetic field; (b) magnetic field strength; (c) ion bulk velocity; (d) electron bulk velocity; (e) electric current density calculated from plasma moments: $J = n_e q(V_i - V_e)$, where n_e is the electron number density, q is the unit charge, and V_i and V_e are the ion and electron bulk velocity, respectively; (f) three components of electric field; and (g) energy conversion rate J·E. Vectors are displayed in the LMN coordinate system.

J·E shown in Figure 3g reaches 50 pW/m^3 within the current sheet. J·E > 0 is a kind of "smoking gun" of reconnection, implying the conversion of magnetic energy to the kinetic and thermal energy of the plasma. This explains the asymmetric magnetic field of the MFR, which had a stronger magnetic field on its tailward edge than that on its earthward edge since the earthward part was dissipated through the reconnection. Similar asymmetric magnetic field structure was associated with two coalescing MFRs and was a key signature to identify MFR coalescence (Zhou et al., 2017).

Furthermore, we performed a first-order Taylor expansion analysis (Fu et al., 2015, 2016) to examine whether the X line (radial null) structure existed in this event. We consider the measurements at 18:56:37.22 UT to reconstruct the magnetic topology around the current sheet. We calculated two parameters for quantifying the uncertainty of the first-order Taylor expansion results, $\eta = |\nabla \cdot \boldsymbol{B}| / \mid \nabla \times \boldsymbol{B} \mid$ and $\xi = |\lambda_1 + \lambda_2 + \lambda_3| / |\lambda|_{max}$, where λ_1, λ_2, and λ_3 are the three eigenvalues of the Jacobian matrix $\delta \boldsymbol{B}$ derived from the four-point measurements, and $|\lambda|_{max}$ is the maximum of them (see Fu et al., 2015, 2016 for more details). At this time, the two parameters are quite small (η = 2.4% and ξ = 5.2%), meaning that the first-order Taylor expansion results should be very accurate. We traced and inverse-traced magnetic field lines to obtain the topology, like

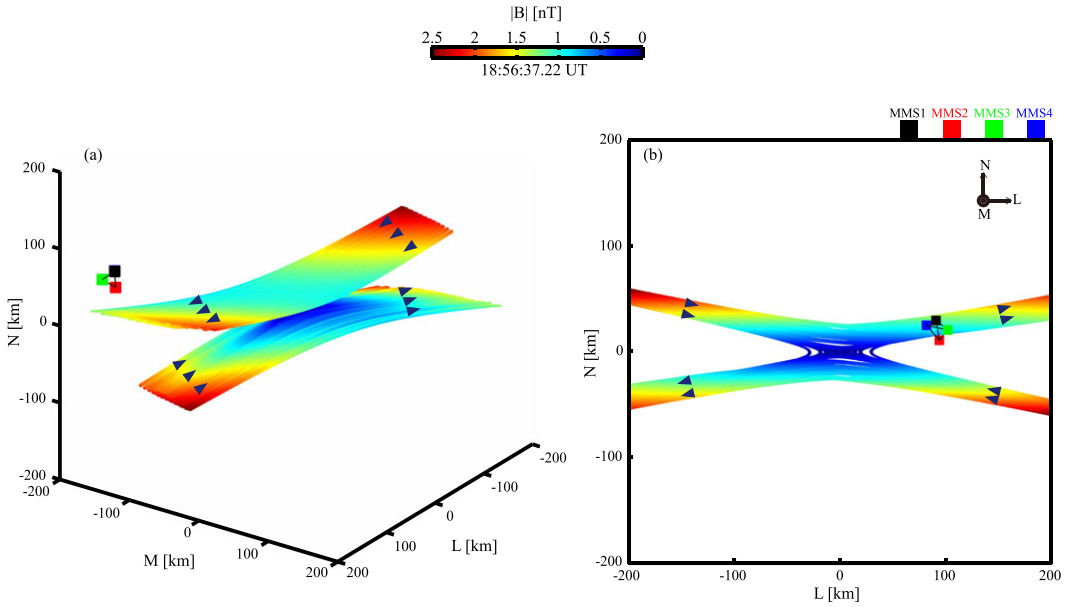

Figure 4. Reconstruction of null point and magnetic field lines near MMS at 18:56:37.22 UT. (a) Three-dimensional field line topology in the LMN coordinate system. (b) Two-dimensional view of this topology along the **M** direction. The colors represent the magnitude of magnetic field while the blue arrows denote the magnetic field directions. The squares mark the four MMS spacecraft.

that done in previous studies (Chen et al., 2018; Fu et al., 2017). Figure 4 presents such topology in the LMN coordinates, with the colors denoting the magnetic field strength and the blue arrows denoting the magnetic field direction. Specifically, Figure 4a shows the topology in 3-D regime, while Figure 4b is a 2-D view of this topology along the **M** direction. Clearly, we see an "X line" structure around the MMS spacecraft (Figure 4b). The angle between the two separatrices of this X line is ~15°, indicating a reconnection rate of nearly 0.1 (Liu et al., 2017). We noticed that the MMS tetrahedron was merely 150 km~0.4 d_i away from the null point, indicating that MMS crossed the diffusion region of this reconnecting current sheet.

3. Discussion and Summary

One interesting question is how long this reconnection persisted. Duration of the reconnection depends on the two parameters: the total magnetic energy stored in the leading part of the MFR (negative B_z) and the energy conversion rate. Here we estimate the magnetic energy stored in the MFR by assuming that the MFR was initially in force-free state. Hence, the azimuthal magnetic field component B_φ is given by $B_0J_1(\alpha r)$, where B_0 is the magnetic field strength at the MFR center, J_1 is the Bessel function of the first kind, α is a constant, and r is the radial distance from origin of the MFR (Lepping et al., 1990). B_0 = 20 nT is derived from the equation $B_0J_1(\alpha R_1) = -6$, where -6 is the magnitude of B_z at the leading edge of the dissipated MFR and R_1 is the distance between the MFR origin and the leading edge. R_1 is estimated as 3,200 km by multiplying the normal speed of the current sheet and the duration of the negative B_z. Total magnetic energy stored within the leading part of the MFR is given by $\lambda_M\int_0^{R_0}\frac{B_\varphi(r)^2}{2\mu_0}\pi r dr$, where R_0 is the radius of the MFR and λ_M is the length of MFR along its axis. $R_0 \approx$ 6,100 km is derived by solving the equation $B_0J_1(\alpha R_0) = -10$, where -10 is the initial azimuthal magnetic field B_z at the leading edge of the MFR for a symmetric reason. Substituting these parameters into the above equation, we found that the total magnetic energy stored in the leading part of the MFR was 1,420 λ_M J.

Assuming that J·E was uniform in a cuboid containing the reconnection site, energy conversion per second by the reconnection is $<J\cdot E>\lambda_L\lambda_M\lambda_N$, where λ_N~100 km is the width of the current sheet, λ_L is the length of the current sheet and can be approximated as 1,000 km by assuming a dimensionless reconnection rate of 0.1 (Liu et al., 2017). According to Figure 3g, the average energy conversion rate $<J\cdot E>$ within the dissipation

layer is about 20 pW/m^3; hence, the total energy conversion rate is 2 λ_M J/s. Therefore, to consume the energy within the leading part of the MFR requires 1,420 λ_M/2 λ_M = 710 s. Multiplying the time and the moving speed of the MFR, which was estimated by the timing analysis, we get 160 km/s × 710 s ≈ 17.8 R_E. This means that the MFR had moved approximately 17.8 R_E before its leading part was entirely eroded. Since B_z at the leading edge is –6 nT, we estimated that it took about 645 s to erode the B_z from −10 to −6 nT. Based on this, as well as the propagation velocity of the MFR, we derived the source location of this MFR as [X, Y] ≈ [−33.5, 10.3] R_E.

Surprisingly, MMS did not detect the ion jet associated with this reconnection. The distance between MMS and the null point (illustrated in Figure 4) was less than one ion inertial length. Thus, MMS was in the ion diffusion region where ion bulk speed was much smaller than the upstream Alfvén speed since ions were demagnetized and not yet accelerated to the Alfvénic speed (Shay et al., 2001). This is the well-known Hall region where electrons are still frozen-in and carry the current. One other possibility is that ions did not response to this reconnection process. It is suggested that ions cannot be involved in the reconnection if the current sheet length is below a threshold (Phan et al., 2018; Wang et al., 2018). In this case, the length of the current sheet is estimated as 1,000 km~3 d_i, which may be too small for ions to be involved.

In summary, we present the first in situ evidence, to the best of our knowledge, for the reconnection between a MFR and the geomagnetic field. The reconnection occurred in a subion-scale thin current sheet between the MFR and the dipole field and was characterized by the super-Alfvénic electron outflow, Hall magnetic and electric field, magnetic energy conversion J·E > 0, and magnetic null point. Since the reconnection started about 10 min before it was observed by MMS (~18:57 UT), it was unlikely responsible for triggering this substorm because the *AE* index was nearly 160 nT 10 min before it was observed. This fast-moving reconnection site in fast flows may contribute significantly to the energy transport and conversion in the magnetotail. Results reported here are relevant to other planets having global magnetic field, where flux ropes and dipolarization fronts have been detected in their magnetotail, such as Saturn and Mercury (Arridge et al., 2015; Jackman et al., 2014; Smith et al., 2017).

Acknowledgments
We thank the fruitful discussion with Yu Lin and Xueyi Wang. We appreciate the MMS teams for the high-quality data and successful operation. This work is supported by the National Natural Science Foundation of China (NSFC) under grants 41522405, 41774154, and 41331070. The data used in this study were obtained from the MMS Science Data Center (https://lasp.colorado.edu/mms/sdc/public/).

References

Arridge, C. S., Eastwood, J. P., Jackman, C. M., Poh, G.-K., Slavin, J. A., Thomsen, M. F., et al. (2015). Cassini in situ observations of long duration magnetic reconnection in Saturn's magnetotail. *Nature Physics*, *12*, 268–271.

Birn, J., Drake, J. F., Shay, M. A., Rogers, B. N., Denton, R. E., Hesse, M., et al. (2001). Geospace Environmental Modeling (GEM) Magnetic Reconnection Challenge. *Journal of Geophysical Research*, *106*, 3715. https://doi.org/10.1029/1999JA900449

Borg, A. L., Øieroset, M., Phan, T. D., Mozer, F. S., Pedersen, A., Mouikis, C., et al. (2005). Cluster encounter of a magnetic reconnection diffusion region in the near-Earth magnetotail on September 19, 2003. *Geophysical Research Letters*, *32*, L19105. https://doi.org/10.1029/2005GL023794

Burch, J. L., Moore, T. E., Torbert, R. B., & Giles, B. L. (2016). Magnetospheric Multiscale overview and science objectives. *Space Science Reviews*, *199*(1–4), 5–21. https://doi.org/10.1007/s11214-015-0164-9

Chen, X. H., Fu, H. S., Liu, C. M., Cao, D., Wang, Z., Dunlop, M. W., et al. (2018). Magnetic nulls in the reconnection driven by turbulence. *The Astrophysical Journal*, *852*(1), 17. https://doi.org/10.3847/1538-4357/aa9991

Daughton, W., Scudder, J., & Karimabadi, H. (2006). Fully kinetic simulations of undriven magnetic reconnection with open boundary conditions. *Physics of Plasmas*, *13*(7), 072101.

Deng, X. H., Matsumoto, H., Kojima, H., Mukai, T., Anderson, R. R., Baumjohann, W., & Nakamura, R. (2004). Geotail encounter with reconnectiondiffusion region in the Earth's magnetotail: Evidence of multiple X lines collisionless reconnection? *Journal of Geophysical Research*, *109*, A05206. https://doi.org/10.1029/2003JA010031

Dere, K. P., Brueckner, G. E., Howard, R. A., Michels, D. J., & Delaboudiniere, J. P. (1999). LASCO and EIT observations of helical structure in coronal mass ejections. *The Astrophysical Journal*, *516*(1), 465–474. https://doi.org/10.1086/307101

Drake, J. F., Shay, M. A., & Swisdak, M. (2008). The hall fields and fast magnetic reconnection. *Physics of Plasmas*, *15*(4), 042306. https://doi.org/10.1063/1.2901194

Drake, J. F., Swisdak, M., Schoeffler, K. M., Rogers, B. N., & Kobayashi, S. (2006). Formation of secondary islands during magnetic reconnection. *Geophysical Research Letters*, *33*, L13105. https://doi.org/10.1029/2006GL025957

Ergun, R. E., Holmes, J. C., Goodrich, K. A., Wilder, F. D., Stawarz, J. E., Eriksson, S., et al. (2016). Magnetospheric multiscale observations of large-amplitude, parallel, electrostatic waves associated with magnetic reconnection at the magnetopause. *Geophysical Research Letters*, *43*, 5626–5634. https://doi.org/10.1002/2016GL068992

Fermo, R. L., Drake, J. F., & Swisdak, M. (2012). Secondary magnetic islands generated by the Kelvin-Helmholtz instability in a reconnecting current sheet. *Physical Review Letters*, *108*(25), 255005. https://doi.org/10.1103/PhysRevLett.108.255005

Fu, H. S., Cao, J. B., Vaivads, A., Khotyaintsev, Y. V., Andre, M., Dunlop, M., et al. (2016). Identifying magnetic reconnection events using the FOTE method. *Journal of Geophysical Research: Space Physics*, *121*, 1263–1272. https://doi.org/10.1002/2015JA021701

Fu, H. S., Khotyaintsev, Y. V., Vaivads, A., André, M., & Huang, S. Y. (2012). Occurrence rate of earthward-propagating dipolarization fronts. *Geophysical Research Letters*, *39*, L10101. https://doi.org/10.1029/2012GL051784

Fu, H. S., Khotyaintsev, Y. V., Vaivads, A., Retinò, A., & André, M. (2013). Energetic electron acceleration by unsteady magnetic reconnection. *Nature Physics*, *9*(7), 426–430. https://doi.org/10.1038/nphys2664

Fu, H. S., Vaivads, A., Khotyaintsev, Y. V., André, M., Cao, J. B., Olshevsky, V., et al. (2017). Intermittent energy dissipation by turbulent reconnection. *Geophysical Research Letters*, *44*, 37–43. https://doi.org/10.1002/2016GL071787

Fu, H. S., Vaivads, A., Khotyaintsev, Y. V., Olshevsky, V., André, M., Cao, J. B., et al. (2015). How to find magnetic nulls and reconstruct field topology with MMS data? *Journal of Geophysical Research: Space Physics*, *120*, 3758–3782. https://doi.org/10.1002/2015JA021082

Huang, C., Lu, Q., Guo, F., Wu, M., Du, A., & Wang, S. (2015). Magnetic islands formed due to the Kelvin-Helmholtz instability in the outflow region of collisionless magnetic reconnection. *Geophysical Research Letters*, *42*, 7282–7286. https://doi.org/10.1002/2015GL065690

Huang, S. Y., Vaivads, V., Khotyaintsev, Y., Zhou, M., Fu, H. S., Retinò, A., et al. (2012). Electron acceleration in the reconnection diffusion region: Cluster observations. *Geophysical Research Letters*, *39*, L11103. https://doi.org/10.1029/2012GL051946

Huang, S. Y., Zhou, M., Yuan, Z. G., Fu, H. S., He, J. S., Sahraoui, F., et al. (2015). Kinetic simulations of secondary reconnection in the reconnection jet. *Journal of Geophysical Research: Space Physics*, *120*, 6188–6198. https://doi.org/10.1002/2014JA020969

Jackman, C. M., Slavin, J. A., Kivelson, M. G., Southwood, D. J., Achilleos, N., Thomsen, M. F., et al. (2014). Saturn's dynamic magnetotail: A comprehensive magnetic field and plasma survey of plasmoids and traveling compression regions and their role in global magnetospheric dynamics. *Journal of Geophysical Research: Space Physics*, *119*, 5465–5494. https://doi.org/10.1002/2013JA019388

Lee, L. C., & Fu, Z. F. (1985). A theory of magnetic-flux transfer at the Earth's magnetopause. *Geophysical Research Letters*, *12*(2), 105–108.

Lepping, R. P., Jones, J. A., & Burlaga, L. F. (1990). Magnetic field structure of interplanetary magnetic clouds at 1 AU. *Journal of Geophysical Research*, *95*(A8), 11,957–11,965. https://doi.org/10.1029/JA095iA08p11957

Lindqvist, P. A., Olsson, G., Torbert, R. B., King, B., Granoff, M., Rau, D., et al. (2016). The spin-plane double probe electric field instrument for MMS. *Space Science Reviews*, *199*(1–4), 137–165. https://doi.org/10.1007/s11214-014-0116-9

Liu, Y.-H., Hesse, M., Guo, F., Daughton, W., Li, H., Cassak, P. A., & Shay, M. A. (2017). Why does steady-state magnetic reconnection have a maximum local rate of order 0.1? *Physical Review Letters*, *118*, 085101.

Lu, S., Lu, Q., Lin, Y., Wang, X., Ge, Y., Wang, R., et al. (2015). Dipolarization fronts as earthward propagating flux ropes: A three-dimensional global hybrid simulation. *Journal of Geophysical Research: Space Physics*, *120*, 6286–6300. https://doi.org/10.1002/2015JA021213

Ma, Z. W., & Lu, X. Q. (2009). An island coalescence scenario for near-Earth current disruption in the magnetotail. *Chinese Physics Letters*, *26*(8), 089401.

Phan, T. D., Eastwood, J. P., Shay, M. A., Drake, J. F., Sonnerup, B. U. Ö., Fujimoto, M., et al. (2018). Electron magnetic reconnection without ion coupling in Earth's turbulent magnetosheath. *Nature*, *557*(7704), 202–206. https://doi.org/10.1038/s41586-018-0091-5

Pollock, C., Moore, T., Jacques, A., Burch, J., Gliese, U., Saito, Y., et al. (2016). Fast plasma investigation for Magnetospheric Multiscale. *Space Science Reviews*, *199*(1–4), 331–406. https://doi.org/10.1007/s11214-016-0245-4

Ruffenach, A., Lavraud, B., Owens, M. J., Sauvaud, J. A., Savani, N. P., Rouillard, A. P., et al. (2012). Multispacecraft observation of magnetic cloud erosion by magnetic reconnection during propagation. *Journal of Geophysical Research*, *117*, A09101. https://doi.org/10.1029/2012JA017624

Runov, A., Angelopoulos, V., Sitnov, M. I., Sergeev, V. A., Bonnell, J., McFadden, J. P., et al. (2009). THEMIS observations of an earthward-propagating dipolarization front. *Geophysical Research Letters*, *36*, L14106. https://doi.org/10.1029/2009GL038980

Russell, C. T., Anderson, B. J., Baumjohann, W., Bromund, K. R., Dearborn, D., Fischer, D., et al. (2016). The Magnetospheric Multiscale magnetometers. *Space Science Reviews*, *199*(1–4), 189–256. https://doi.org/10.1007/s11214-014-0057-3

Russell, C. T., & Elphic, R. C. (1979). ISEE observations of flux transfer events at the dayside magnetopause. *Geophysical Research Letters*, *6*(1), 33–36. https://doi.org/10.1029/GL006i001p00033

Russell, C. T., Mellott, M. M., Smith, E. J., & King, J. H. (1983). Multiple spacecraft observations of interplanetary shocks: Four spacecraft determination of shock normals. *Journal of Geophysical Research*, *88*(A6), 4739–4748. https://doi.org/10.1029/JA088iA06p04739

Shay, M. A., Drake, J. F., Rogers, B. N., & Denton, R. E. (2001). Alfvénic collisionless magnetic reconnection and the hall term. *Journal of Geophysical Research*, *106*(A3), 3759–3772. https://doi.org/10.1029/1999JA001007

Shay, M. A., Drake, J. F., & Swisdak, M. (2007). Two-scale structure of the electron dissipation region during collisionless magnetic reconnection. *Physical Review Letters*, *99*(15), 155002. https://doi.org/10.1103/PhysRevLett.99.155002

Slavin, J. A., Lepping, R. P., Gjerloev, J., Fairfield, D. H., Hesse, M., Owen, C. J., et al. (2003). Geotail observations of magnetic flux ropes in the plasma sheet. *Journal of Geophysical Research*, *108*(A1), 1015. https://doi.org/10.1029/2002JA009557

Smith, A. W., Slavin, J. A., Jackman, C. M., Poh, G.-K., & Fear, R. C. (2017). Flux ropes in the Hermean magnetotail: Distribution, properties, and formation. *Journal of Geophysical Research: Space Physics*, *122*, 8136–8153. https://doi.org/10.1002/2017JA024295

Sonnerup, B. U. Ö., & Scheible, M. (1998). Minimum and maximum variance analysis. In *Analysis Methods for Multi-Spacecraft Data*, edited by G. Paschmann, and P. W. Daly, ISSI scientific Report SR-001 (pp. 185–220). Bern, Switzerland: International Space Science Institute.

Vogiatzis, I. I., Isavnin, A., Zong, Q. G., Sarris, E. T., Lu, S. W., & Tian, A. M. (2015). Dipolarization fronts in the near-earth space and substorm dynamics. *Annales de Geophysique*, *33*(1), 63–74. https://doi.org/10.5194/angeo-33-63-2015

Wang, R., Lu, Q., Du, A., & Wang, S. (2010). In situ observations of a secondary magnetic island in an ion diffusion region and associated energetic electrons. *Physical Review Letters*, *104*(17), 175003. https://doi.org/10.1103/PhysRevLett.104.175003

Wang, R., Lu, Q., Nakamura, R., Baumjohann, W., Huang, C., Russell, C. T., et al. (2018). An electron-scale current sheet without bursty reconnection signatures observed in the near-earth tail. *Geophysical Research Letters*, *45*, 4542–4549. https://doi.org/10.1002/2017GL076330

Wang, R., Lu, Q., Nakamura, R., Huang, C., du, A., Guo, F., et al. (2016). Coalescence of magnetic flux ropes in the ion diffusion region of magnetic reconnection. *Nature Physics*, *12*(3), 263–267. https://doi.org/10.1038/nphys3578

Winglee, R. M., Harnett, E., & Kidder, A. (2009). Relative timing of substorm processes as derived from multifluid/multiscale simulations: Internally driven substorms. *Journal of Geophysical Research*, *114*, A09213. https://doi.org/10.1029/2008JA013750

Zhang, T. L., Lu, Q. M., Baumjohann, W., Russell, C. T., Fedorov, A., Barabash, S., et al. (2012). Magnetic reconnection in the near Venusian magnetotail. *Science*, *336*(6081), 567–570. https://doi.org/10.1126/science.1217013

Zhong, Z. H., Tang, R. X., Zhou, M., Deng, X. H., Pang, Y., Paterson, W. R., et al. (2018). Evidence for secondary flux rope generated by the electron Kelvin-Helmholtz instability in a magnetic reconnection diffusion region. *Physical Review Letters*, *120*(7), 075101. https://doi.org/10.1103/PhysRevLett.120.075101

Zhou, M., Ashour-Abdalla, M., Deng, X., Schriver, D., El-Alaoui, M., & Pang, Y. (2009). THEMIS observation of multiple dipolarization fronts and associated wave characteristics in the near-Earth magnetotail. *Geophysical Research Letters*, *36*, L20107. https://doi.org/10.1029/2009GL040663

Zhou, M., Berchem, J., Walker, R. J., el-Alaoui, M., Deng, X., Cazzola, E., et al. (2017). Coalescence of macroscopic flux ropes at the subsolar magnetopause: Magnetospheric Multiscale observations. *Physical Review Letters*, *119*(5), 055101. https://doi.org/10.1103/PhysRevLett.119.055101

Zhou, M., Berchem, J., Walker, R. J., El-Alaoui, M., Goldstein, M. L., Lapenta, G., et al. (2018). Magnetospheric Multiscale observations of an ion diffusion region with large guide field at the magnetopause: Current system, electron heating and plasma waves. *Journal of Geophysical Research: Space Physics*, *123*, 1834–1852. https://doi.org/10.1002/2017JA024517

Zhou, M., Deng, X., Tang, R., Pang, Y., Xu, X., Yuan, Z., & Huang, S. (2014). Evidence of deflected super-Alfvénic electron jet in a reconnection region with weak guide field. *Journal of Geophysical Research: Space Physics*, *119*, 1541–1548. https://doi.org/10.1002/2013JA019556

Zhou, M., Pang, Y., Deng, X., Huang, S., & Lai, X. (2014). Plasma physics of magnetic island coalescence during magnetic reconnection. *Journal of Geophysical Research: Space Physics*, *119*, 6177–6189. https://doi.org/10.1002/2013JA019483

Zong, Q. G., Fritz, T. A., Pu, Z. Y., Fu, S. Y., Baker, D. N., Zhang, H., et al. (2004). Cluster observations of earthward flowing plasmoid in the tail. *Geophysical Research Letters*, *31*, L18803. https://doi.org/10.1029/2004GL020692